OFFICE OF CIVILIAN RADIOACTIVE WASTE MANAGEMENT
SPECIAL INSTRUCTION SHEET

1. QA: N/A

Complete Only Applicable Items

This is a placeholder page for records that cannot be scanned or microfilmed

2. Record Date	3. Accession Number
10/01/2000	MOL.20010319.0379
4. Author Name(s)	**5. Author Organization**
A. Ramirez, et al	Lawrence Livermore National Laboratory

6. Title
Electrical Imaging at the Large Block Test Yucca Mountain, Nevada

7. Document Number(s)	8. Version
UCRL-JC-140906	N/A
9. Document Type	**10. Medium**
REPORT	Optic/Paper

11. Access Control Code
Public

12. Traceability Designator
RPR #27443

13. Comments
This document contains One-of-a-Kind color pages which can be located through the Records Processing Center

Electrical Imaging at the Large Block Test—Yucca Mountain, Nevada

A. Ramirez and W. Daily

Lawrence Livermore National Laboratory
Livermore, CA 94550
October 2000

Abstract

A monolithic block of densely welded tuff was excavated from a site on Fran Ridge near Yucca Mountain, Nevada so that coupled thermohydrological processes could be studied in a controlled, in situ experiment. A series of heaters were placed in a horizontal plane about 3 m from the top of the 3 m by 3 m by 4.5 m high block. Temperatures were measured at many points within and on the block surface and a suite of other measurements were taken to define the thermal and hyrologic response. Electrical resistance tomography (ERT) was used to map 2 dimensional images of moisture content changes along four planes in the block.

The ERT images clearly delineate the drying and wetting of the rockmass during the 13 months of heating and subsequent six months of cool down. The main feature is a prominent dry zone that forms around the heaters then gradually disappears as the rock cools down. Other features include linear anomalies of decreasing moisture content which are fractures dehydrating as the block heats up. There are also examples of compact anomalies of wetting. Some of these appear to be water accumulation in fractures which are draining condensate from the block. Others may be rain water entering a fracture at the top of the block . During cool-down a general rewetting is observed although this is less certain because of poor data quality during this stage of the experiment.

Introduction

The United States Department of Energy (DOE) is investigating the suitability of Yucca Mountain as a potential site for the nation's first high-level nuclear waste repository. The site is located about 120 km northwest of Las Vegas, Nevada. Favorable aspects of Yucca Mountain as a potential repository site include its arid nature and the sorptive properties of the rock. The arid environment results in unsaturated conditions at the potential emplacement horizon, which is the Topopah Spring Tuff of the Paintbrush Group. The major advantages of unsaturated conditions are that container corrosion, waste-form leaching, and radionuclide transport mechanisms are minimized because there is less available water to contact the waste package.

Because a repository is required to isolate radioactive wastes for long periods of time, the evaluation of that isolation is unprecedented. Specifically, evaluation must be made of the

isolation potential of the repository system composed of both natural and engineered components for 10,000 years. Complex processes that must be considered include hydrologic processes in unsaturated fractured porous rock as well as the significant processes that will result from the introduction of heat generated by radioactive decay of the waste.

Because of the long time frames that must be evaluated, it will be impossible to directly measure the performance except for very small portions of the entire waste/natural system interactions. Therefore, analysis based on conceptual models using computer codes to evaluate or predict the performance will be the basis for determining the potential for the repository to properly function (that is, to provide isolation) over the long times required. Such an analysis entails more than merely achieving a scientifically believable view of the repository. It must provide sufficient rigor in evaluation of the models and assumptions to be useful in a regulatory process wherein the analysis will be subject to challenge by those opposed to the project. Thus, the models need to be tested and verified to the extent possible.

A testing strategy has been developed that is designed to evaluate the models by accelerating portions of the testing to address different segments of the time frames of interest and to look at the functional relationships of different geometric scales. Because no single test can address all of the issues several different test approaches are being used to assess the models. The types of test, identified in order from the smallest geometric scale to the largest, and generally from the shortest duration to the longest, fall into the following categories:

1-Laboratory tests of core-size samples. These are tests to measure matrix properties and processes and properties of single fractures. The duration of such tests is usually a few hours or days.

2-Laboratory tests of approximately 1 m scale block samples (small block tests). These samples are large enough to allow testing of fracture properties, the effects of discontinuities and even some multiple-fracture responses. They provide an understanding of the processes of a fractured rock and enable the development of functional relationships in terms of the influence of scale.

3-Field tests on large blocks of approximately 4 m scale. These tests are critical because of the sufficient size to incorporate a fracture system that is representative of the distribution of fracture dimensions and characteristics that would likely be in a repository—with the possible exception of major geologic structures, such as faults. A single test of this scale has been conducted.

4-In situ tests of scale tens of meters. These are relatively large tests that involve hundreds of cubic meters and extend for many months or years. They incorporate sufficient volumes of rockmass to be representative of total rock-mass responses. These tests have boundary conditions that are poorly controlled and thus are focused more on hypotheses testing for processes that are scale-dependent and on characterization of repository rock behavior. Whereas these tests last several years, they are nonetheless highly accelerated, in comparison with the rates and processes expected in an actual repository.
5-Confirmation tests. These tests do not involve issues of scale, because the actual repository and its associated process rates will be monitored. Thus one of the purposes of such testing is to confirm that the testing performed at smaller scales and abbreviated time frames accurately reflect or predict the behavior of the system.

Of course, many techniques are used to monitor conditions in these various tests depending on the time and spatial scale of the test and the limitation of the measurement method. One method, which has been used in several of these tests, is electrical resistance tomography (ERT). We describe here use of ERT in the Large Block Test (LBT) which is an in situ test of type 3 described above. This test was conducted on an outcrop of Topopah Spring tuff on the east side of Fran Ridge.

The major objective of the LBT is to study the coupled thermal-hydrologic-mechanical processes in a rock sample large enough to contain realistic fracturing and other heterongeniety. Several different measurements were being made by researchers at Lawrence Livermore National Laboratory (which include electrical resistance tomography and neutron logging) to determine movement of moisture, to determine rock mass deformation and to analyze the temperature field in the rock. In support of these field activities, thermo-hydrologic modeling was also done.

Description of the Block and Instrumentation

An outcrop area at Fran Ridge was selected to be the site for the LBT because of the suitable rock type exposed and accessibility of the site. A 3 m X 3 m X 4.5 m block of fractured nonlithophysal Topopah Spring tuff was isolated. Figure 1 shows the block, partially exposed for fracture mapping, prior to installation of test and monitoring instrumentation.

Instruments and heaters were installed within and on the surface of the block. The instruments installed in the block included resistance temperature devices (RTD) to measure

temperatures, electrodes to conduct electrical resistivity tomography (ERT), Teflon liners for the neutron logging in boreholes, Humicaps to measure relative humidity, pressure transducers to measure gas phase pressure, conventional and optical multiple point borehole extensometers (MPBX) for measuring displacements along boreholes, fracture gauges mounted across fractures on the block surface to monitor fracture deformation,

To create a one-dimensional thermal field within the block heaters were placed in the rock 1.75 m from the base to simulate a plane heat source, and an aluminum plate fitted with heating/cooling coils was mounted on the top of the block. This plate was connected to a heat exchanger to allow thermal control of the top surface at approximately 60°C. The heaters were 450 Watts each and were installed in each of the five horizontal heater holes. The heaters were turned on February 28, 1997 and turned off on March 10, 1998. Data were collected during cool-down until September 30, 1998.

Electrical Resistance Tomography

ERT is a geophysical imaging technique which can be used to map subsurface resistivity (Daily and Owen, 1991). The ERT measurements consist of a series of voltage and current measurements from buried electrodes using an automated data collection system. The data are then processed to produce electrical resistivity tomographs. Electrical resistance tomography (ERT) was proposed independently by Henderson and Webster (1978) as a medical imaging tool and by Lytle and Dines (1978) as a geophysical imaging tool. The technique has been actively developed for medical imaging (e.g., Isaacson, 1986; Barber and Seager,1987; Yorkey *et al.*, 1987). Early adaptations of the technique to the field of geophysics were by Pelton *et al.*, (1978), Dines and Lytle (1981), Tripp *et al.* (1984), Wexler *et al.*, (1985), Oldenburg and Li (1994), Sasaki (1992), Daily and Owen (1991), and LaBrecque *et al.*(1996b).

Here we describe briefly some of the important features of the two dimensional (2D) algorithm used for ERT. The algorithm (see LaBrecque *et al.*; 1996a) solves both the forward and inverse problems. The forward problem is solved using a finite element technique in two dimensions. The inverse problem implements a regularized solution that minimizes an objective function. The objective of the inverse routine is to minimize the misfit between the forward modeling data and the field data, and a stabilizing functional of the parameters. The stabilizing functional is the solution roughness. This means that the inverse procedure tries to find the smoothest resistivity model that fits the field data to a

prescribed tolerance. Resistivity values assigned in this way to the finite element mesh constitute the ERT image. Although the mesh is of a large region around the electrode arrays, only the region inside the ERT electrode array is used in the calculations of moisture content and reported here because the region outside the array is poorly constrained by the data.

To calculate the changes in the rock's electrical resistivity we compared a data set obtained after heating started, and a corresponding data set obtained prior to heating. One may consider subtracting, pixel by pixel images from these two different conditions. However, this approach could not be used because the resistivity structure is three-dimensional. The finite element forward solver cannot generate a model that will fit the data so the code chooses a solution with a poor fit. Our experience is that these effects can be reduced by inverting the quantity

(1)

$$\frac{r_a}{r_b} \times r_h$$

where r_a is the measured transfer resistance after heating started, r_b is the transfer resistance before heating and r_h is the calculated transfer resistance for a model of uniform resistivity. This approach tends to reduce the effects of anomalies which do not satisfy the 2D assumptions of the resistivity model because the 3D effects tend to cancel in the ratio since they are contained in both terms r_a and r_b.

Changes in Moisture Content

Resistivity of the rock is influenced by changes in moisture content, porosity, cation exchange capacity, solutes in the pore water, and temperature. In the following analysis we assume that only moisture content and temperature are important. It is likely that porosity and cation exchange capacity change very little during the test. Ionic content of the pore water will change as steam forms and condenses. Of course, mineral solubility will also depend on temperature. However, we have no data about how these mechanisms are affecting pore fluid at each point in the rock and so we must make a simplifying assumption

that pore water conductivity is constant. An increase in temperature or moisture causes a resistivity decrease. However, near the heater there may be regions where the increasing temperature, decreasing pore water resistivity, is opposed by the rockmass drying which increases the resistivity. Our goal in this section is to use the images of resistivity change near the heater, along with the measured temperature field and what is known of initial conditions in the rockmass to estimate moisture change during heating.

In order to estimate moisture content changes, we need to account for both effects of temperature, measured at many points by temperature sensors, and resistivity changes, measured by ERT. This is possible by either using laboratory data establishing the relations between moisture, temperature and resistivity or by using a suitable model of electrical conduction in porous media. Roberts and Lin (1997) have published data on the resistivity of Topopah Spring tuff as a function of moisture content. There is, however, limited data on temperature dependence (only below 95 C) so that direct use of this relationship is not possible.

On the other hand, Waxman and Thomas (1974a,b) describe a model for electrical conduction in partially saturated shaly sands typical of oil reservoirs (intended for oil field data) which accounts for conduction through the bulk pore water as well as conduction through the electrical double layer near the pore surface (see also Vinegar and Waxman, 1984). This model can predict temperature dependence of the resistivity but several of the model parameters are empirically determined and not available for tuff. Roberts and Lin (1997) suggest that the Waxman model provides reasonably good estimates of resistivity for saturations greater than 20%. For saturations less than 20%, their data shows that the Waxman Smits model substantially underpredicts the resistivity. We will use this model to account for the temperature effects on the resistivity changes and to estimate changes in rock saturation.

Waxman and Thomas begin with a parallel circuit model for conductance

$$C = \frac{1}{F^*}(C_W + BQ_V) \qquad (2)$$

where C is the conductivity or 1/R where R is the resistivity

F^* is the formation factor or ϕ^{-m} where ϕ is the porosity and m the porosity exponent,

C_W is the pore water conductivity,

B is the equivalent conductance of counter ions on the double layer,

Q_V is the effective concentration of exchange cations.

The first term represents conductance through the bulk pore water while the second term is the conductance along the double layer. This expression can be modified for partially saturated media by realizing that the first term is just Archie's equation and $Q/S = Q_V$ where S is the fractional saturation. In terms of resistivity, equation 2 can be re-written as:

$$R = \frac{R_w \phi^{-m} S^{1-n}}{S + R_w B Q} \qquad (3)$$

where the exponent n is approximately 2, the saturation index in Archie's modified equation, and R_W is the water resistivity. Waxman and Thomas (1974a,b) reported results that suggest that m is approximately equal to n. When $R_W BQ \gg S$ the electrical double layer is the primary conduction pathway. When $R_W BQ \ll S$, the primary conduction pathway is through the open pore space.

We can use equation 3 in ratio form in order to calculate resistivity changes in the form of resistivity ratios. When the primary conduction pathway is through the water in the open pore space, the resistivity ratio can be calculated as:

$$\frac{R_a}{R_b} = \frac{R_{w,a}}{R_{w,b}} \left(\frac{S_b}{S_a} \right)^2 \qquad (4)$$

where are the resistivities before and after heating started, $R_{W,b}$ and $R_{W,a}$ are the water resistivities before and after heating. S_b and S_a are the saturations before and after heating started; we will refer to this case as model 1. This equation implies that the temperature

dependence of the resistivity change is proportional to the change in water resistivity caused by temperature increases.

When the primary conduction pathway is through the electrical double layer, the ratio form of equation 3 simplifies to:

$$\frac{R_a}{R_b} = \frac{S_b}{S_a}\frac{B_b}{B_a} \qquad (5)$$

where B_b and B_a are the equivalent conductances of counter-ions in the electrical double layer; we will refer to this case as model 2. This equation implies that the temperature dependence of the resistivity ratio is caused by changes in counter-ion conductance due to temperature changes. Comparing equations 4 and 5, we see that the resistivity changes caused by saturation changes are largest for model 1 where the primary conduction pathway is through the pore space. We note that neither of these two models accounts for changes in water resistivity caused by rock/water chemical interactions. If chemical reactions cause changes in the concentration or types of ions in the water, or change the porosity due to mineral precipitation or dissolution, the estimated saturation changes will be in error.

We used the available temperature data to construct temperature maps along each ERT image plane. It is necessary to have a reliable temperature measurement for each area (each tomograph pixel) where we wish to calculate the saturation change.

The ERT images provide a measure of change from baseline resistivity R (through the resistivity ratio). Equations 4 and 5 can be used to relate electrical resistivity changes to changes in saturation when the temperatures are known and the temperature dependence of R_W and B can be calculated.

Calculation of changes in volumetric water content requires rock porosity and initial saturation values. Initial values of block saturation were calculated from neutron logs in 4 boreholes. The water saturation from all of these holes agrees and shows values ranging from about 60% to 90% by pore volume (Wilder *et al.*, 1997). We assume a uniform initial saturation of 75% and a porosity of 12%.

Since the magnitude of R_WBQ is changing in space and time we have chosen to estimate the changes in saturation by using both model 1 and 2. This approach should provide bounds to the domain of possible saturations that may be present. However, there is some reason to believe that welded tuff should show behavior closer to model 2 than to model 1. This can be seen by assuming average values of cation exchange capacity for welded tuff of about 3 meq/100 g, porosity of 0.10 (porosity is used to calculate Q) and R_W =39 ohm-m at 25°C (resistivity of J-13 water). For these values R_WBQ is about 23 at 25° C and it increases with temperature. Since S is bounded by 0.0 and 1.0, then $R_WBQ >> S$ and the primary pathway for conduction is the electrical double layer. However, if the cation exchange capacity, porosity or water resistivity varied significantly across the ERT image plane, it is possible that model 1 results are closer to reality.

In fact, we believe that model 1 is more representative of the rock mass for two reasons. First, the saturation estimates based on this model are in better agreement with those of the neutron log where that data are available. Second, the saturation estimates based on model 2 occasionally predict S> 1.0 which, of course, is non physical.

Results

ERT data was taken from four planar arrays in the block before the heaters were turned on. Two horizontal planes of electrodes were arranged on the surface, azimuthally around the block. One plane was approximately 1.25 m above the heater plane and the other was approximately 1.25 m below the heater plane. The two other planes were vertical, dividing the block into four quadrants . The vertical planes were sampled from electrode arrays on the side of the block and a single vertical array at the center of the block. The electrode arrangement is shown in Figure 2.

At the intersection of these ERT planes there should be agreement and this is the case for the vertical planes because they share a common electrode array along that intersection. Such agreement is not very good for the intersection of the vertical and horizontal planes. Complete agreement cannot be expected in these cases for two reasons:

First, the spatial distribution of sensitivity and resolution is different for the vertical and horizontal planes because of the difference in how they are sampled by the electrodes. The sampling scheme was a direct result of normal experimental constraints. As a result, however, the two planes will tend to resolve features differently. The common electrode

array in the vertical planes produces good resolution where they intersect and this is why they tend to agree. In general two sided sampling as in the vertical planes leaves a low sensitivity region along the top and bottom. On the other hand, the all-around sampling of the horizontal planes leaves a low sensitivity region in the center where we shall see that agreement with the vertical planes is poorest.

Second, in all of these images we are trying to reconstruct a three-dimensional target using a model that is strictly two-dimensional. This means that the ERT algorithm finds the best finite element model for the resistivity structure of the block that fits the data within a given criterion. Unfortunately, it only can choose from models where the resistivity is constant orthogonal to the image plane (the two dimensional assumption in the ERT model). It picks the best model but it cannot be the correct model. That model chosen for two different planes will be different, especially if the planes are perpendicular as the vertical and horizontal planes are here.

We note here that some of the resistivity images reconstructed late in the experiment (and the moisture changes inferred from them) are questionable because of the sparse data. As the rockmass dehydrated and the resistivity increased dramatically, the data quality declined. Fewer usable data results in a poorly constrained reconstruction which might look smeared or washed out. This is particularly noticeable in the vertical planes beginning early in 1998.

The result of interpreting the changes in resistivity tomographs in terms of changes in moisture content are shown in Figures 3 and 4. Blank image planes indicate data which did not converge to an ERT solution or no data were collected. The 2D orthogonal planes shown in Figures 3 and 4 don't provide a full description of the 3D block but they do show spatial relationships that might not be available from the other geophysical data.

We will first discuss the results in terms of conceptual behavior—rock drying, condensate accumulation in fractures, and loss of condensate out of the block. The goal is to determine the impact that heterogenieties (such as fractures) have on the distribution and fate of water in the block. We begin with a discussion of the horizontal planes.

Horizontal Planes

The obvious result shown in the horizontal planes (see Figure 3) is that changes in moisture content initially are very small and increase in magnitude and extent as the test proceeds.

Notice, however, that there are some asymmetries between the two cases. Through 6/25/97 (117 days into heating) the upper plane (plane above the heater elevation) shows significantly less change from initial conditions than the lower plane. As early as 4/22/97 (53 Days into heating) a strong and compact wetting anomaly appears below the heaters. It remains visible at 5/22/97 (30 days later) but then disappears from subsequent images until 11/19/97, when it reappears and persists to the end of the test on 3/19/98. We believe that this feature results from a major fracture, or fracture system, intersecting the image plane and that in April and May, condensate from the heated region, finds its way to this fracture and moves by gravity down the conduit and out of the block. Once the source is drained, the anomaly goes away. The source of the water from November through March is less certain but may be condensate.

There are only two other strong indications of saturation increasing in these planes. The one on 8/26/97 (perhaps persisting to 9/24/97) near the north edge of the lower image plane, also behaves like a water-wet fracture—spatially compact; developing quickly and then going away. The other anomaly, on 2/24/98 in the north west corner of the upper image plane, does not look like the draining of water through a fracture. We do not know the cause of this feature.

The other characteristic of images in both planes are zones of drying which start to appear as early as 5/22/97 in the lower plane. Clearly, this drying is a result of the high temperatures but the effects recorded in these images appear different above and below the heater plane. Above the heater, drying appears later and appears to form anomalies with rounded outlines. Below the heater, the anomalies appear as early as May, are more localized, and are linear in shape. The linear shape may be caused by the matrix drying around a planar fracture that cuts through the image plane. A good example of this is the feature running diagonally from south-west corner to the north-east corner between 5/22/97 and 3/19/98. Even though the anomaly changes character throughout this period it probably arises from the same structure in the rockmass—a fracture or system of fractures.

Other anomalies of dehydration occur in both planes—some are quite prominent and some are minor. They all support the notion that the dehydration front is steadily advancing from the heater plane into both image planes but that the process is heavily controlled by rockmass heterogeneities.

Vertical Planes

The vertical image planes (see Figure 4) intersect the heater plane and even more clearly delineate the effects of heating the block. Early in the test dehydration does not seem to be centered on the heaters as might be expected. Laboratory experiments indicate that fractured tuff does not dry uniformly (Daily *et al.*, 1987) but starts along the fracture surfaces and proceeds into the intact matrix. The small amounts of dehydration observed before 5/22/97 (about 83 days into the heating) are likely a result of such rock heterogeniety.

Later in the test, when larger volumes of intact matrix are dry, a continuous dry zone forms around the heaters and once formed, it is the dominant feature in both vertical image planes all the way through the last data of cool down (3/19/98)(see Figure 4). For example, on 5/22 and 6/25 in the south to north plane, zones of drier rock are centered on two heaters. After 6/25 these individual zones have coalesced into a single continuous dehydrated zone which grows in size with some locations eventually losing 85% of the original water content (saturation ratio 0.15). This large dry zone around the heater persists until late cool-down in March of 1998 when it appears to be breaking up.

Once formed, the heater dry zone is not a smooth planar anomaly reflecting the heater geometry. Instead it is very irregular in shape with many appendages. There is also a tendency for the dry zone to be relatively flat on top and bottom early in the test but convex on top and concave on the bottom late in the test. We do not have a hypothesis for this behavior. We believe that this rugose image of the heated zone is the result of rock heterogenities such as fractures. Consider, for example, the part of the block located above the heaters in the western half of the West to East plane. By 5/22/97 there is a vertically oriented dry zone forming between the heater plane and the top of the block. Four months later (9/24/97) it is a very linear anomaly that looks a lot like dehydration along a vertical fracture intersecting both the heater plane and the image plane. In Figure 5 the interpolated temperature field is superimposed on the 7/23/97 and the 1/23/98 saturation images. Notice that this linear looking zone in the ERT reconstruction corresponds to a high temperature anomaly—additional evidence for drying along a vertical fracture or fractured zone. This figure also demonstrates an approximate correspondence between the dehydration as defined by the ERT data and the 100° C isotherm.

During one month of high block temperatures—8/26/97 to 9/24/97—there is a saturation anomaly adjacent to the dryer feature discussed above. We believe that this combination

could be from drying along a nearly vertical fracture zone and wetting of adjacent rock which may be evidence for a heat pipe effect.

Rain fell during the test on 9/2/97 (day 186). The amount and duration of rain is unknown so that the more important data, how much rain water got through the covering and onto the block itself, is also unknown. In addition, rain fell a few kilometers from the site on 6/12/97 and may have also fallen at the site. The temperature data provide evidence that some water reached the block because on that date a RTD 5 cm above the heater registered a sharp drop in temperature from about 120 C to 100 C. No such temperature drop was observed below the heaters. This temperature data is consistent with water moving quickly along a fracture from the top to deep within the block.

The RTD that experienced the temperature excursion possibly linked to the rain infiltration is only about 50 cm from the west-east ERT image plane and 25 cm from the south-north ERT plane. In the 6/25/97 data there is no clear evidence of increased saturation at this location in the west-east plane. In the closer south-north plane, however, the projection of that RTD location onto the plane correlates precisely with the bottom of the strong moisture anomaly in the image (see figure 4). Unfortunately, this identification is not so simple because this same anomaly appears in the May 22nd image, before the rainfall, and appears to evolve in the July August and September images, after the rainfall. It is possible that these ERT anomalies represent a region of fractured rock where both condensate (in May) and meteoric water (in June) collect and the July August and September images show this trapped moisture being driven out the top of the block (9/24/97 image).

Comparison of ERT and Fracture Distribution

The ERT images show ample evidence that the block is behaving like a heterogeneous system and the most obvious source of heterogeneity is fracturing. Of course, the block is heavily fractured and those fractures were mapped at the five exposed surfaces. Unfortunately, a search for fractures that might be responsible for the ERT anomalies is complicated by two problems. First, fractures are not planar so that the surface expression may be only a guide to the fracture location inside the block. Second, the fracture density is so high that almost any anomaly can be matched with a fracture making such an association of little value.

Undaunted by these facts we made an attempt to see a correlation between fractures and anomalies in the ERT images. We chose ERT anomalies that were large in magnitude and

persistent over several months and tried to match these with fractures which mapped continuously on two or more faces of the block and that appeared approximately planar . We could not see a consistently convincing correlation between the surface fractures and ERT image anomalies.

Comparison of ERT and Neutron Logs

Neutron logs were made in five vertical holes in the block and from this data the moisture content calculated along each borehole at 12 times during heating. In Figure 6 we compare the ERT moisture estimates with the neutron log data from the vertical borehole nearest to the west to east vertical ERT plane. Of course, the main feature in both data is the development of a large dehydrated zone around the heater that grows from 1 m to 2 m thick in the six months time covered by the data. Notice that from both of these measurements a maximum change in water content near the heaters is calculated to be about 70%. This close agreement is significant since the neutron log and ERT are two completely independent measurements .

There are also differences in the inferences about moisture content from the two methods. For example, the neutron data seems to indicate a slightly thicker dry zone around the heaters. Less subtle, however, are the comparisons outside the heated region. The neutron log does not indicate any significant wetting above the baseline condition anywhere in the block. On the other hand ERT points to several zones of enhanced wetting. This difference implied by the two results is important because the fate of condensate water is important to understanding the water budget of the block during the test.

We believe that some condensate is stored in the block. However, while the neutron probe is insensitive to it, ERT is probably overly sensitive to its presence. This results from the water distribution in the rockmass. As a matrix block dries, the steam moves into a fracture, then down the pressure gradient along fracture until it reaches the dew point where it condenses. Since the matrix there is already nearly saturated (typically 80%) and also has a very low permeability (typically a few micro Darcey), the condensate remains in the fracture aperture. Because the fracture porosity is small compared to the matrix porosity the neutron probe correctly measures very little increase in moisture content at the location of this condensate. On the other hand, electric current can easily sample fracture networks because, when wet, they act as a network of highly conducting pathways. Therefore, ERT is overly sensitive to this small volume fraction of water and may over estimate the saturation when water is present in a fracture network.

On the other hand both methods are sensitive to dehydration of the block. The heat load drives large volumes of vapor from the pores of matrix blocks. This changes the amount of water in volumes comparable to the integration volume of the neutron probe so that this log is sensitive to the change. Matrix water loss also affects electrical current flow which happens along paths through the connected pore water in the matrix.

In figure 6 the neutron log shows slight drying relative to baseline in the top 2 meters of the block. This may be a response to the vertically oriented drying zone seen in the ERT images only 50 cm from the neutron logging hole.

Summary and Discussion

We believe that the ERT images along with the other data we have discussed support a simple and physically realistic conceptual model for the hydrothermal behavior of the system during the Large Block Test:

1-Dehydration around the heaters is progressive, producing first a small hot zone which grows larger and dryer as time progresses. This is the principal process observed and is driven by the imposed heat load. [This thermally driven dehydration is the central theme of Figure 4.] The effect is approximately one dimensional, evolving with time along the vertical axis of the block. However, deviation from a uniformly one dimensional moisture distribution is significant and appears to be controlled by hererogeneity in the block--probably fractures. [For example, the heated zone is not imaged by ERT as a strictly planar anomaly. Even more obvious is the especially strong feature in the west to east plane forming as early as May 1997 and persisting to February 1998. This is a large, strong and persistent dry zone extending from the heater plane upward to the top of the block.]

2-Water in matrix pores vaporizes as temperature rises. Evaporation must occur even below boiling but become especially rapid at the boiling point which is about 96 °C.

3-Water vapor first leaves pores adjacent to fractures because the pressure gradient is steepest there. Then the drying front progresses into the matrix block until the whole block is in equilibrium between the suction potential and the vapor pressure. [ERT sees many linear features of high resistivity that are likely dehydration along fractures and systems.]

4-Once in the fracture, the water vapor is highly mobile and moves quickly down the pressure gradient. Some of this vapor will exit the block, especially through the top because it is not sealed like the block sides

5- That portion of the vapor that remains in the block will move down the pressure gradient, losing heat as it goes, until the dew point is reached at which point it condenses. This condensate rapidly fills the fracture aperture. [Such saturated fractures provides a network of conducting pathways for electrical current in the rock that weren't initially present and ERT sees this network as an increase in electrical conductivity. Interpretation of this change results as an unnecessarily large moisture increase. This water is detected as a small perturbation by neutron probe because the fracture porosity accounts for a small part of the rock and the tool is insensitive to it because of the volumetric averaging of the measurement.]

6- The behavior and fate of this condensate that forms in fractures is the key to repository performance since it is this water, if it can seep back into the emplacement drift, that is most likely to determine the useful lifetime of the canisters—the longer this water can be kept away from the canisters, the longer they will survive.

(a) This water may drain out of the system-through the bottom of the block. This is especially likely below the heaters. [Notice the moisture anomaly below the heater near the center of the west to east plane in July 1997. It becomes weaker in the January 1998 as though it is a fracture draining.] However, drainage may also occur for water above the heaters, especially during the early part of the test before the boiling isotherms coalesce from individual heaters. In fact, even a well-developed boiling isotherm may be overwhelmed by large water volumes moving in fractures. This possibility is equivalent to the seepage of water back into the emplacement drift of the repository. Rain water may have provided such an event on 6/12/97 and 9/2/97. [Notice that in the July 1997 south to north plane there is a linear feature of high saturation—rain water and/or condensate--that is poised above a gap in the dehydration zone forming around the heated plane. The arrangement suggests fracture drainage may be keeping this zone near the heaters from drying.]

(b) This water may participate in a heat pipe above the heaters. [During August and September of 1997, directly above the heaters, there is a

persistent wet anomaly adjacent to a persistent dry anomaly in the west to east plane. This may be the ERT signature for a heat pipe.]

(c)This water may remain immobile, held by capillarity. [There are several persistent wet zones imaged in Figure 4 which may exemplify this effect.]

(d)This water may be imbibed into the matrix by the forces of capillary suction. (This seems unlikely to be an important fate of free water because of the short lifetime of this test since, very small permeability of the matrix and the relatively low suction potential of the initially wet matrix.)

Acknowledgements—*This work was supported by the Office of Civilian Nuclear Waste Isolation. The field work for the large block test was led by Wunan Lin of Lawrence Livermore National Laboratory.*

This work was performed under the auspices of the U.S. Department of Energy by Lawrence Livermore National Laboratory under contract W-7405-ENG-48. This work is supported by the Yucca Mountain Site Characterization Project, LLNL.

References

Barber, D. C. and A. D. Seagar, Fast reconstruction of resistance images, Clinical Physics and Physiological Measurement, *8, Suppl. A,* 47-55, 1987.

Daily, W. and E. Owen, Cross-borehole resistivity tomography, *Geophysics, 56,* 1228-1235, 1991.

Daily, W., W. Lin and T. Buscheck, Hydrological properties of Topopah Spring tuff: Laboratory measurements, *J. Geophysical Res., 92,* No B8, 7854-7864, 1987.

Dines, K. A. and R. J. Lytle, Analysis of electrical conductivity imaging, *Geophysics, 46,* 1025-1036, 1981.

Henderson, R. P. and J. G. Webster, An impedance camera for spatially specific measurements of thorax, *IEEE Trans. Biomed, Eng, BME-25,* 250-254, 1978.

Isaacson, D., Distinguishability of conductivities by electric current computed tomography, *IEEE Trans. on Medical Imaging, vol. MI-5,* no. 2, 91-95, June, 1986.

LaBrecque, D. J., Miletto, M., Daily, W., Ramirez, A., and Owen, E., The effects of noise on Occam's inversion of resistivity tomography data: Geophysics, *61,* 538-548, 1996a.

LaBrecque, D. J., A. Ramirez, W. Daily, A. Binley and S. Schima, ERT monitoring of environmental remediation processes: Meas. Sci. Technol., *7,* 375-383, 1996b.

Lytle, R. J. and K. A. Dines, An impedance camera: A system for determining the spatial variation of electrical conductivity, Lawrence Livermore Laboratory, Livermore, California, UCRL-52413, 1978.

Oldenburg, D. W. and Y. Li, Inversion of induced polarization data, Geophysics, vol. 59, no. 9, pp 1327-1341, 1994.

Pelton, W. H., L. Rijo and C. M. Swift, Jr., Inversion of Two-dimensional resistivity and induced-polarization data, *Geophysics, 43,* no. 4, 788-803, June, 1978.

Roberts, J. and W. Lin, Electrical properties of partially saturated Topopah Spring Tuff: Water distribution as a function of saturation, *Water Res. Research, 33,* No. 4, 577-587, April, 1997.

Sasaki, Y., Resolution of resistivity tomography inferred from numerical simulation, *Geophysical Prospecting, 40,* 453-463, 1992.

Tripp, A. C., G. W. Hohmann and C. M. Swift, Two dimensional resistivity inversion, *Geophysics, 49,* 1708-1717, 1984.

Vinegar, H. J. and M. H. Waxman, Induced polarization of shaly sands, *Geophysics, 49,* no. 8, 1267-1287, 1984.

Waxman, M.H. and E. C. Thomas, "Electrical Conductivity's in Shale Sands - I. The Relation Between Hydrocarbon Saturation and Resistivity Index; The Relationship between Hydrocarbon Saturation and Resistivity Index," *Journal of Petroleum Technology* (Feb.) 213-218; Transactions AIME, 257, 1974a.

Waxman, M.H. and E.C. Thomas, "Electrical Conductivities in Shaly Sands - II. The Relation Between Hydrocarbon Saturation and Resistivity Index; II. The Temperature Coefficient of Electrical Conductivity," *Journal of Petroleum Technology* (Feb.) 218-225; Transactions AIME, 257, 1974b.

Wexler, A., B. Fry and M. R. Neuman, Impedance-computed tomography algorithm and system, *Applied Optics, 24,* no. 23, 3985-3992, December, 1985.

Wilder, D., W. Lin, S. C. Blair, T. Buscheck, R. C. Carlson, K. Lee, A. Meike, A. L. Ramireiz, J. L. Wagoner and J Wang, Large block test status report, Lawrence Livermore National Laboratory, UCRL-ID-128776, August, 1997. Chapter 2 page 20

Yorkey, T. J., J. G. Webster and W. J. Tompkins, Comparing reconstruction algorithms for electrical impedance tomography, *IEEE Trans Biomedical Engineering, BME-34,* no. 11, 843-852, November, 1987.

Figure Captions

Figure 1. Photograph of large block site. In this photo the upper portion of the block is exposed to allow mapping of fractures.

Figure 2. Layout of ERT electrodes for the Large Block Test. All electrodes are on the surface of the block except the array in the center where the two vertical planes intersect. The location of the heater holes are shown for reference.

Figure 3. Changes in the distribution of moisture content in two horizontal image planes. Blank spaces indicate data sets that did not converge. The saturation ratio is (moisture content)/(initial moisture content). (a) The upper plane. (b) The lower plane.

Figure 4. Changes in the distribution of moisture content in two vertical image planes. Blank spaces indicate data sets that did not converge. The saturation ratio is (moisture content)/(initial moisture content). (a) The south-north plane. (b) The west-east plane.

Figure 5. Interpolated temperature isotherms (in degrees Celsius) superimposed on ERT-derived images of volumetric water change in the west to east plane. The change in water content was calculated assuming a porosity of 0.12 and an initial saturation of 0.75.

Figure 6. Comparison of neutron log and ERT measurements of changes in moisture content.

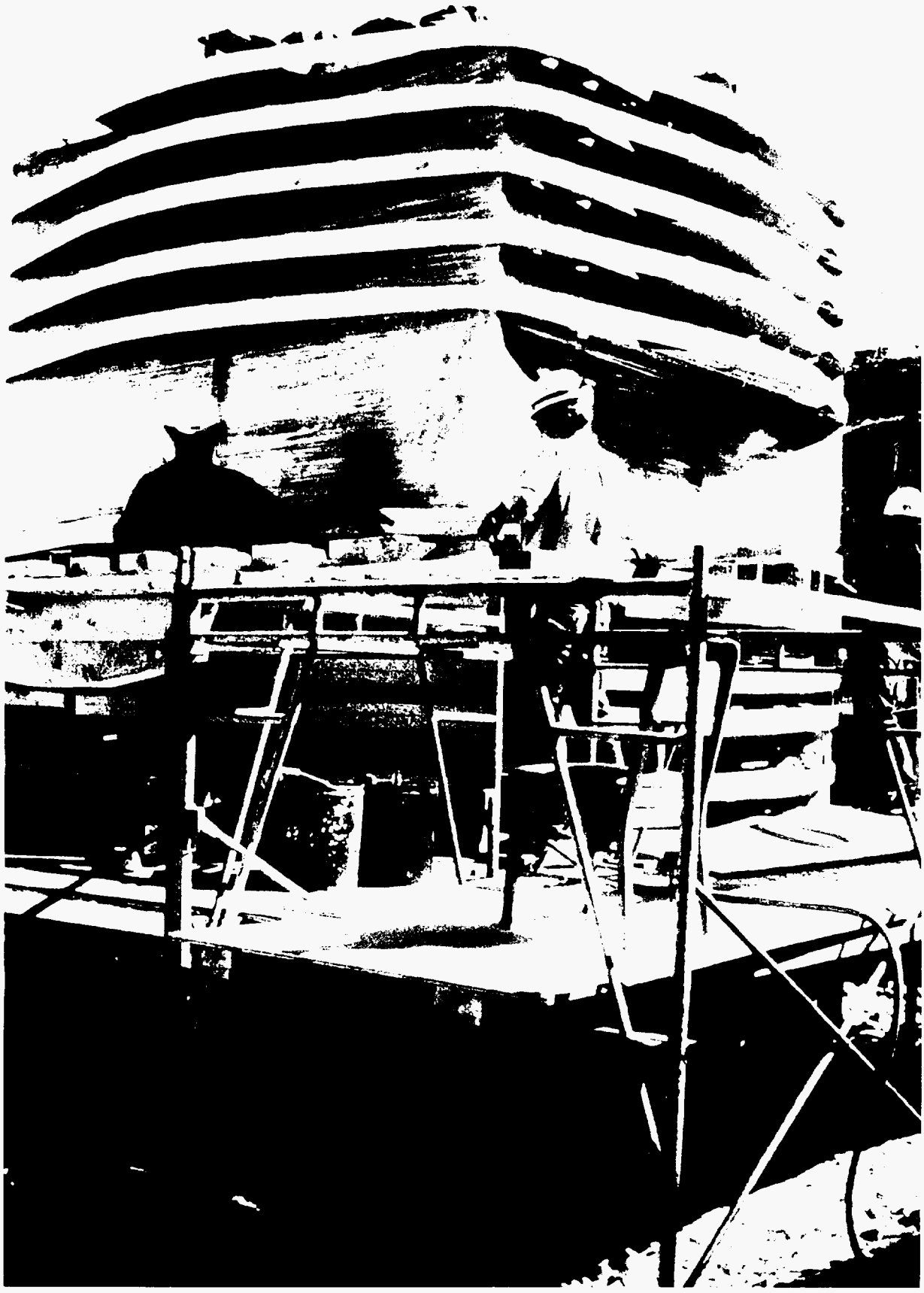

Figure 1

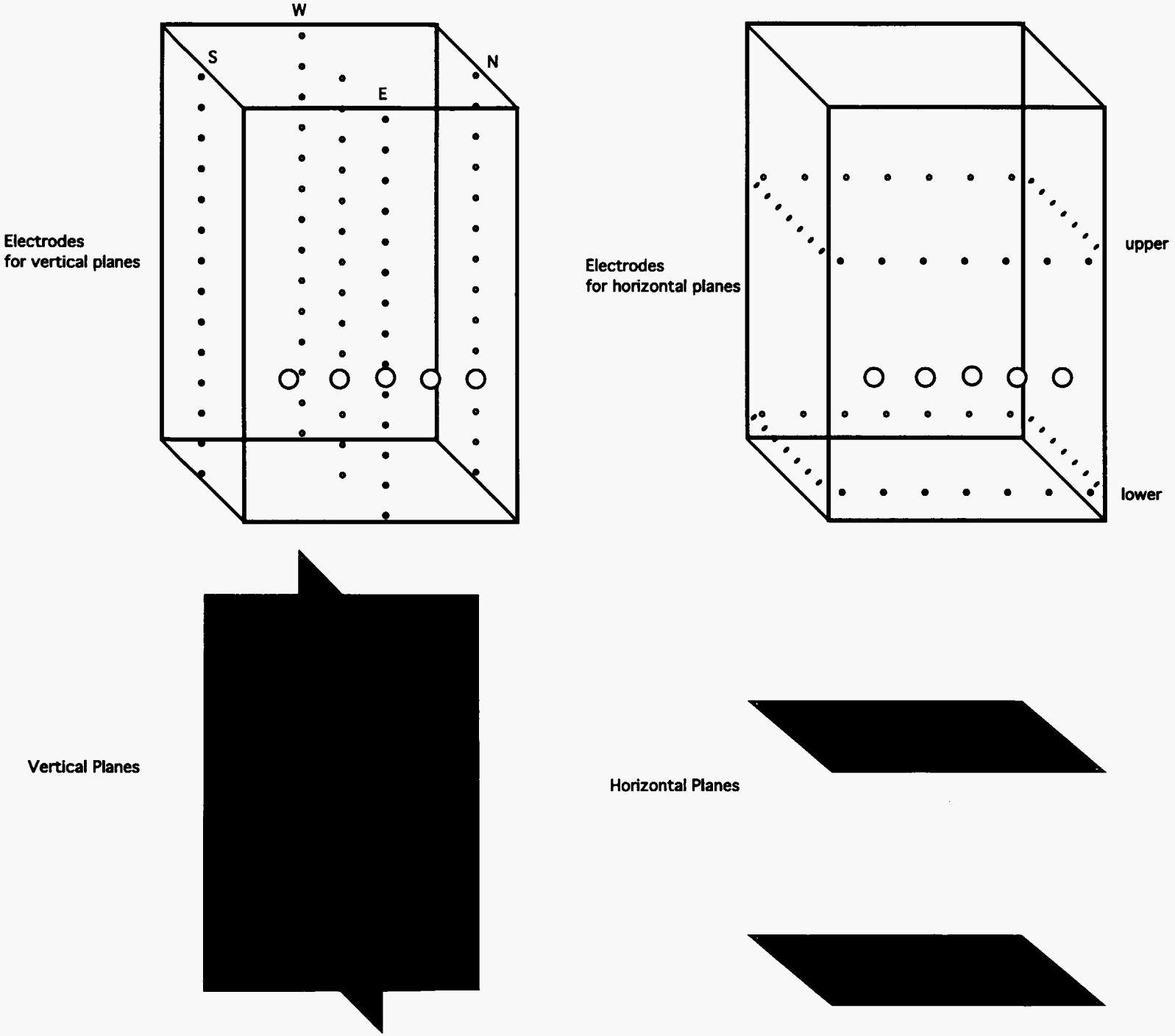
W
S
N
E
Electrodes
for vertical planes
Electrodes
for horizontal planes
upper
lower
Vertical Planes
Horizontal Planes

Figure 2

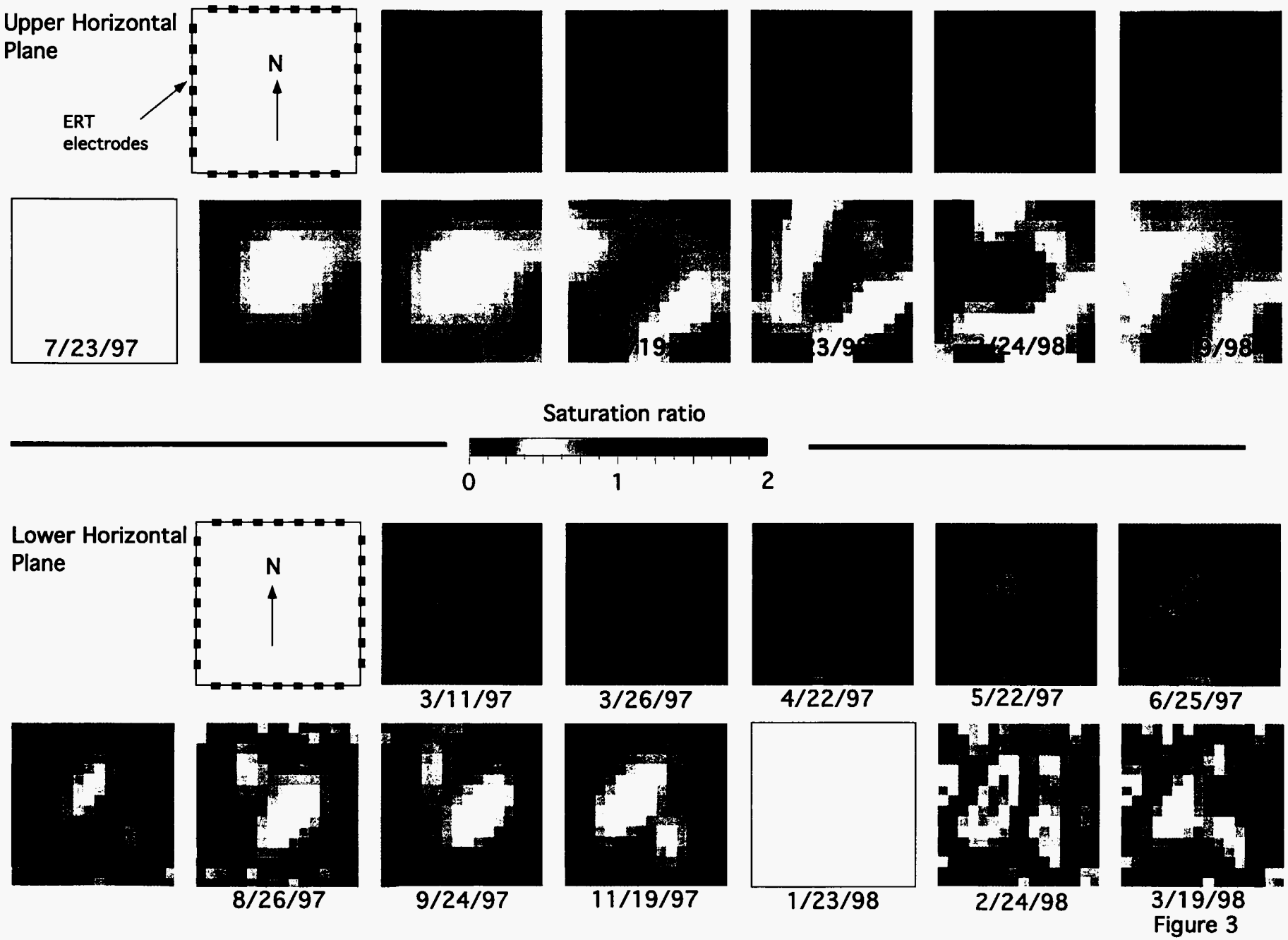
Upper Horizontal Plane
N
ERT electrodes
7/23/97
Saturation ratio
0
1
2
Lower Horizontal Plane
N
3/11/97
3/26/97
4/22/97
5/22/97
6/25/97
8/26/97
9/24/97
11/19/97
1/23/98
2/24/98
3/19/98

Figure 3

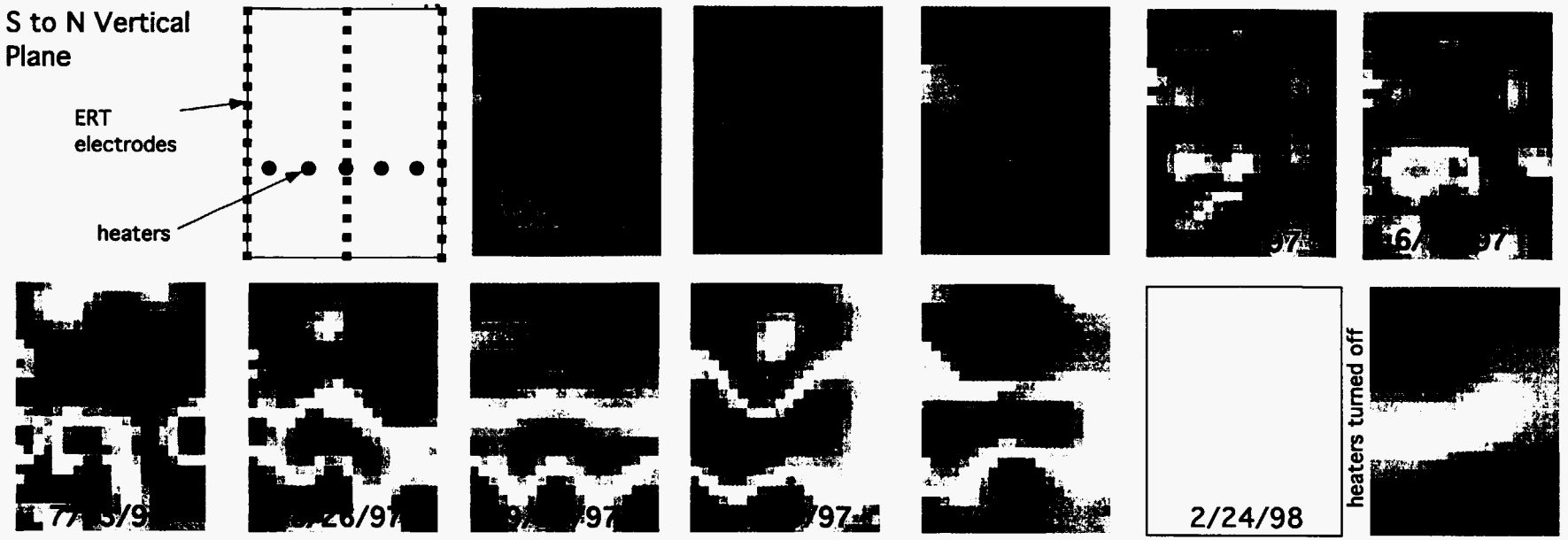

Saturation ratio

0 1 2

Figure 4

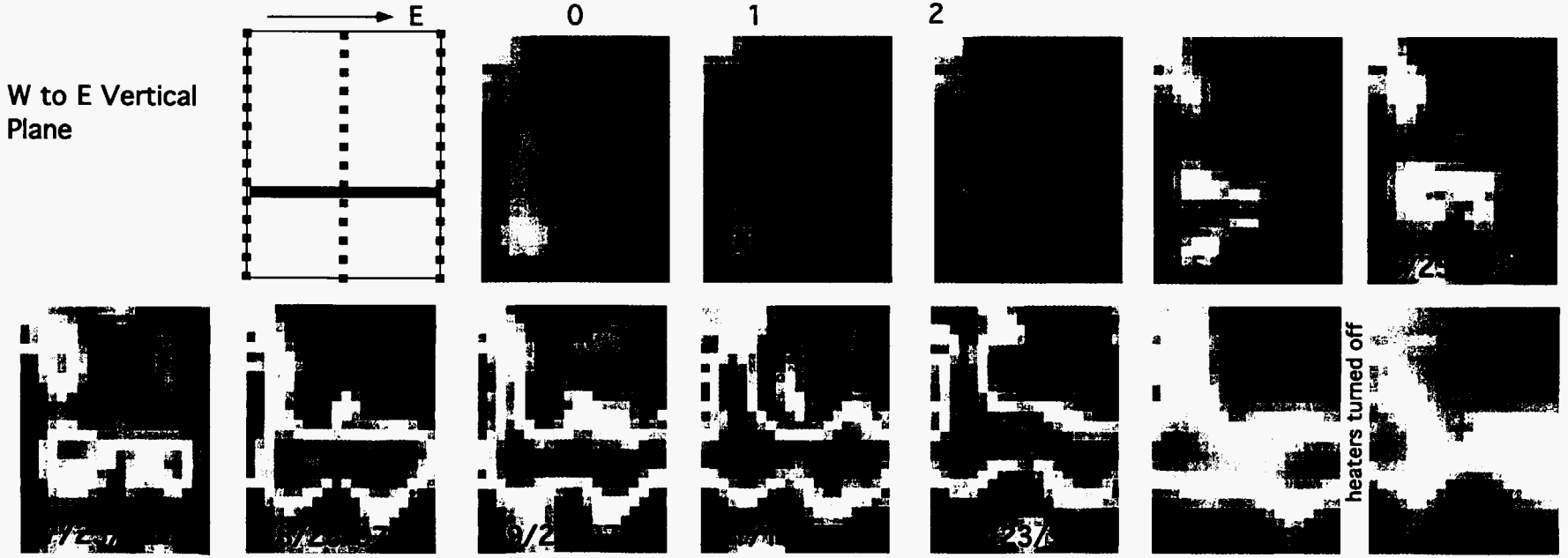

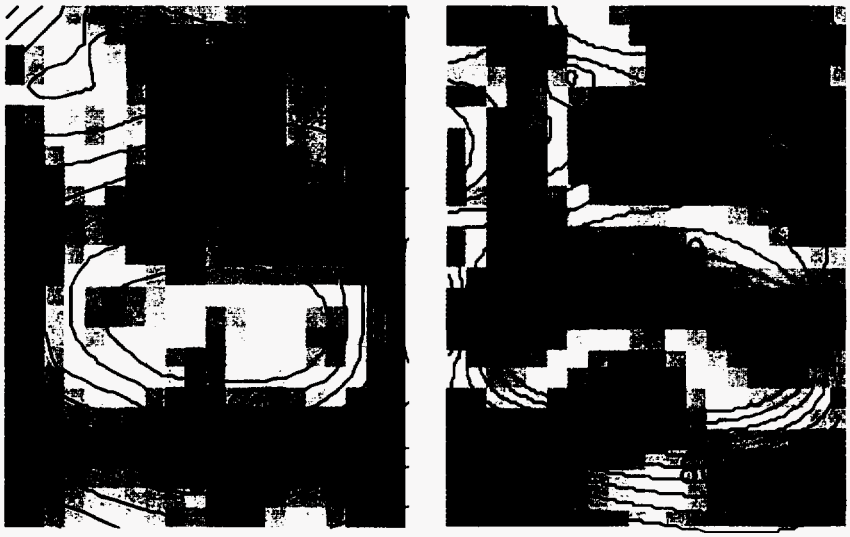

7/23/97 1/23/98

volumetric water difference from baseline
(before heating)

-0.09 0.0 0.09

Figure 5

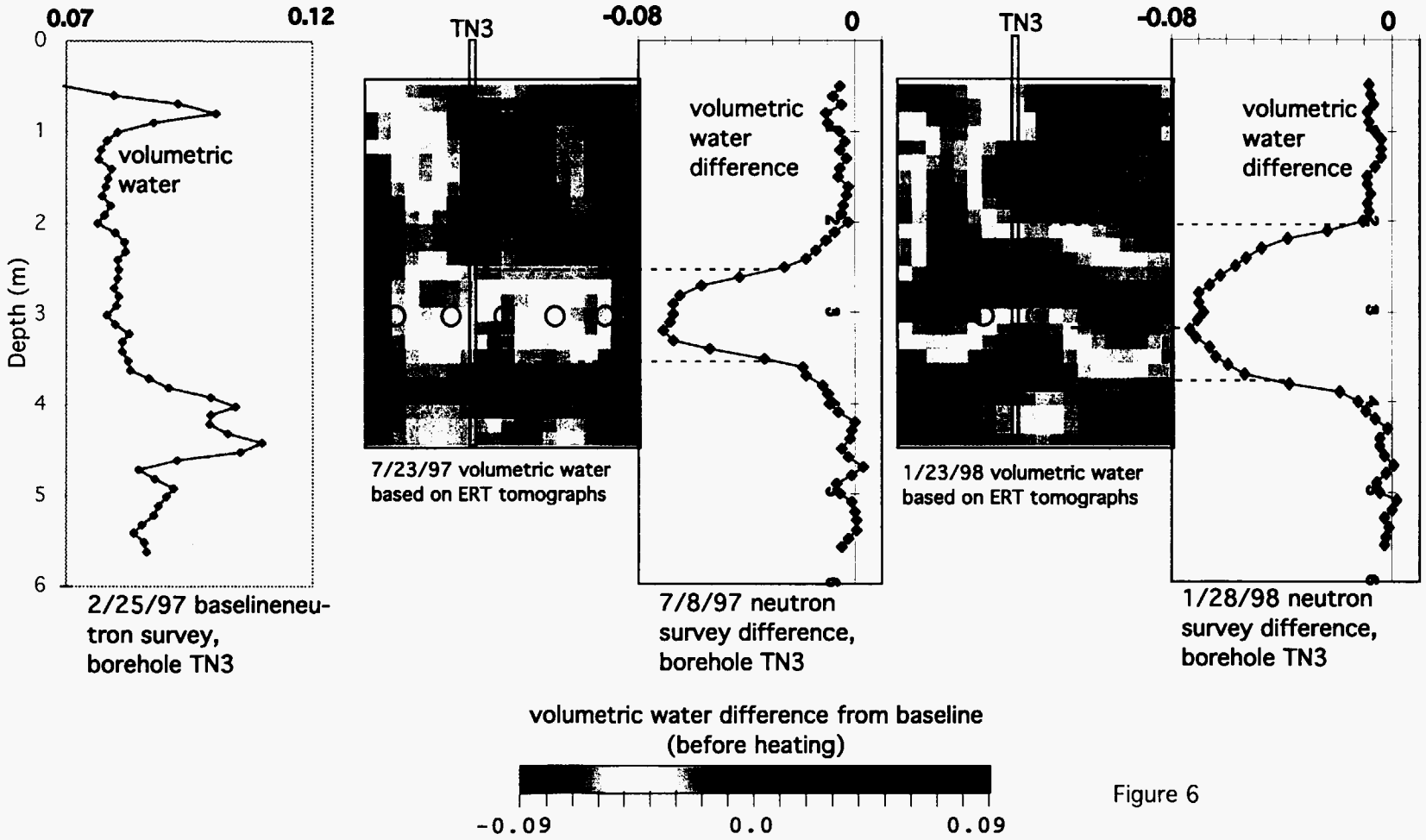
0.07
0.12
0
1
2
3
4
5
6
Depth (m)
volumetric water
2/25/97 baseline neutron survey, borehole TN3
TN3
-0.08
0
volumetric water difference
7/23/97 volumetric water based on ERT tomographs
7/8/97 neutron survey difference, borehole TN3
TN3
-0.08
0
volumetric water difference
1/23/98 volumetric water based on ERT tomographs
1/28/98 neutron survey difference, borehole TN3
volumetric water difference from baseline (before heating)
-0.09
0.0
0.09

Figure 6